FEATURE ARTICLE

A Microscopic View of Laser Ablation

Leonid V. Zhigilei, Prasad B. S. Kodali, and Barbara J. Garrison*

Department of Chemistry, The Pennsylvania State University, 152 Davey Laboratory, University Park, Pennsylvania 16802

Received: October 17, 1997; In Final Form: February 10, 1998

Recent applications of the breathing sphere model for molecular dynamics simulations of laser ablation of organic solids have yielded detailed microscopic data of the processes involved. The results to date include a prediction of a fluence threshold for ablation, an explanation for the presence of clusters in the plume and a consistent analytical description of the velocity distribution for both matrix molecules and heavier analyte molecules in matrix-assisted laser desorption. In this paper we review the approach and the basic physical picture that emerges from the simulations, present new results, and discuss future prospects for microscopic simulations of laser ablation.

I. Introduction

The use of microscopic computer simulations such as molecular dynamics (MD) or Monte Carlo calculations has exploded over the past couple of decades. These simulations allow one to obtain quantitative information such as energy, temperature, pressure, and velocity distributions that are often measured in experiments, as well as qualitative pictures of atomic motions for a plethora of processes.

One field that has barely been explored by such simulations is laser ablation. In these experiments a laser is used to irradiate a sample, causing material to be removed. At first glance it is not apparent that these experiments should be harder to model than experiments using an energized particle beam to remove material, a field in which there are numerous simulations.[1]

There are some critical differences, however. Laser ablation is believed to be a collective effect, rather than a sequence of collisions between atoms or molecules.[2,3] The immediate consequence is that many more particles will be needed in the simulation. As discussed later, some experiments of interest involve molecular solids, and thus the particles of interest are molecules composed of tens to hundreds of atoms. The other difference is time scale. While the shortest laser pulses may be subpicosecond, they are often much longer. The particle removal process including the plume development occurs on an even longer time scale. Thus, laser ablation involves time and length scales too large for conventional microscopic modeling approaches, especially if one wants to run many simulations.

There have been a few attempts, however, to address the laser ablation phenomena by conventional atomic level MD method.[4−8] For a molecular system the dynamics of disruption of the hydrogen bonds[5] and the energy transfer rates between matrix and analyte molecules in matrix-assisted laser desorption[6] were studied. The dependence of the shape of the ablation crater on irradiation regime was addressed in simulations of laser ablation of silicon.[7,8] These works have clearly demonstrated the attractive sides of the MD method. The challenge remains, however, to take these microscopic pictures and translate them into mesoscopic characteristics such as local temperature, pressure, and energy distributions. In addition, the analysis of the ejected plume in terms of velocity, angular, and cluster distributions requires a significantly bigger system and a longer simulation time so that statistically significant data can be obtained.

A molecular dynamics model where a group of atoms rather than each atom is treated as a unit[9−11] was used to explain the differences between ablative photodecomposition and thermal processes in organic polymers. This approach is especially suitable for molecular solids where tightly bound internal structure and weak intermolecular interactions can be treated separately.[12]

Before proceeding to our new microscopic model for laser ablation, we would like to point out some of the diverse array of practical applications of laser ablation. In surgery, this process is used for controlled removal of tissue. Scientific and technological efforts are aimed at achieving more precise control over the ablation depth and minimizing thermal and mechanical damage.[13] In mass spectrometry, laser ablation is used to produce big organic molecules or ions in the gas phase for subsequent mass spectrometric investigations.[14] Recent developments in the matrix-assisted laser desorption ionization (MALDI) technique have dramatically increased the available mass range and possible resolution.[3,15] In this technique the large molecules of interest (i.e., the analytes) are incorporated into a matrix of molecules that readily absorb the incident laser light. Finally, film synthesis by pulsed laser deposition has opened up wide opportunities for producing new and artificially structured materials and coatings.[16]

A number of theoretical studies have been done on laser ablation.[17−23] The complexity and diversity of the processes involved in laser ablation, namely, laser excitation of absorbing molecules, energy transfer from the excited molecules into the internal and translational modes of the solid, material disintegration, and prompt forward ejection, along with processes in the

S1089-5647(97)03378-6 CCC: $15.00
Published on Web 03/24/1998

plume, hinder the analytical description of the phenomenon. Even a qualitative picture of laser ablation has not been established, and analytical models based on such diverse assumptions as the thermofluctuational sublimation of molecules from the surface (surface vaporization)[19,24] and explosive bulk desorption due to a nonequilibrium phase transition[18,23,25] or critical pressure gradient[17,21,22,26] are used to explain the experimental observations.

The current understanding of laser ablation is thus fragmented. There are several qualitative pictures that have led to various analytical models. These models are bounded by an a priori assumption of the desorption/ablation mechanism and, thus, cannot describe the transition between the two regimes nor do they account for the interplay of the different processes involved. Finally, the analytic models do not describe characteristics of the plume such as velocity, angle, and cluster distributions.

Our goal is to develop a comprehensive model that incorporates the fundamental properties of the material and the laser and predicts the events that follow the irradiation of the material. Namely, we would like to accomplish the following:

- Identify the processes that distinguish desorption from ablation.
- Explain a fluence threshold for ablation.
- Predict the cluster distribution in the plume.
- Reveal the physics leading to the velocity distributions of ejected molecules. In particular, the axial velocities are larger than the radial velocities, and thus the angular distributions are forward peaked. In addition, current analytic formulas for the velocity distributions do not always fit experimental data satisfactorily.
- Explain entrainment of large/heavy molecules in plume. In particular, these molecules embedded at low concentrations in a matrix of smaller molecules are found to ablate with nearly the same axial velocities as the matrix molecules.
- Explain ablation processes as a function of laser properties such as laser fluence and pulse width.
- Finally, we would like the model to be sufficiently flexible that inhomogeneous materials and various laser excitation models can be investigated.

We believe that the molecular dynamics approach is an ideal candidate for meeting the above-stated goals. The advantage of the MD method is that only details of the microscopic interactions need to be specified, and no assumptions are made about the character of the processes under study. Moreover, the MD method is capable of providing a complete microscopic description of the dynamical processes involved in laser ablation. As stated above, however, the challenges in using a MD description of laser ablation are the limitations of time and length scales.

We have developed a breathing sphere model aimed at overcoming these limitations.[27−29] The novel feature of the breathing sphere model is an approximate representation of the internal atomic motions that permits a significant expansion of the time and length scales of the model yet still allows one to reproduce a realistic rate of the vibrational relaxation of excited molecules. The initial verification of the model has been performed by simulating the laser ablation for molecular solids. Due to the extensive use of laser ablation of molecular films in mass spectrometry,[3,14,15] a wealth of experimental data is available for comparison with simulation results. We find that the model provides a realistic description of the ablation of molecular films and matrix-assisted laser desorption. Moreover, the simulation results provide insight into the microscopic mechanisms of laser ablation and allow us to discuss the relationship between the physical processes leading to the ablation[27,28] and the final parameters of the ejected material.[29]

A brief description of the proposed breathing sphere model for laser ablation of organic solids is given in section II. Complete details of the model are given in ref 27. Section III presents results from the simulation, and section IV discusses prospects for future simulations.

II. Breathing Sphere Model

The model assumes that each molecule (or appropriate group of atoms) can be represented by a single particle that has the true translational degrees of freedom but an approximate internal degree of freedom. This internal (breathing) mode allows one to reproduce a realistic rate of the conversion of internal energy of the molecules excited by the laser to the translational motion of the other molecules. Because the molecules and not the atoms are the particles of interest, the system size can be significantly larger. Moreover, since explicit atomic vibrations are not followed, the time step in the numerical integration is longer. Below we describe the essential components of the breathing sphere model for laser ablation.

(a) Equations of Motion. The Hamiltion, H, which describes the system is given by

$$H = {}^1/_2\sum_i m_i(\mathrm{d}r_i/\mathrm{d}t)^2 + {}^1/_2\sum_i M_i(\mathrm{d}R_i/\mathrm{d}t)^2 + {}^1/_2\sum_{i,j} U_r(r_i,r_j,R_i,R_j) + \sum_i U_{\mathrm{R}}(R_i) \quad (1)$$

where r_i and R_i are the position and radius of the ith molecule. The mass of the particle is m_i, and the inertia or effective mass of the internal molecular motion is denoted by M_i. The intermolecular potential among the particles is U_{r} and the internal potential is U_{R}, both of which are defined below.

The key difference between this Hamiltonian and that of conventional atomistic MD simulations is the internal coordinate, R_i, with its internal potential, U_{R}. As discussed in section IIc, the internal potential is used to regulate the rate of energy transfer from the excited molecule to the remaining system.

(b) Intermolecular Interactions. The interaction among the organic molecules is assumed to be pairwise additive as

$$U_{\mathrm{r}} = \epsilon_n[\exp\{-2\alpha(r_{ij}^{\,s} - d_0)\} - 2\exp\{-\alpha(r_{ij}^{\,s} - d_0)\}] \quad (2)$$

where $r_{ij}^{\,s} = |r_j - r_i| - R_i - R_j$ with the equilibrium distance d_0 defined as the distance between the edges of the spherical particles rather than their centers. The parameters in the intermolecular potential given in eq 2 are fit to the cohesive energy, vibrational/elastic properties, and sizes of the molecules under investigation. These microscopic properties also determine the macroscopic quantities such as speed of sound, thermal conduction, strength, and plasticity of the material.

This prescription for the intermolecular interactions was developed for organic solids. The choice of equilibrium distance at the edges of the spheres is based on the physical concept that the sublimation or cohesive energy of an organic solid is governed primarily by the interaction among atoms on the outside of the molecule. This description allows an easy means of simulating a multicomponent organic solid without introduction of additional specific potentials for different types of organic molecules (i.e., matrix, analyte (big), and photofragmented (small)).

The choice of intermolecular potential can readily be changed for heterogeneous systems. Thus one can conceive of using

potentials appropriate for mixtures of strongly and weakly bound components as in tissue[21,30] or other complex materials.

(c) Rate of Energy Transfer. As mentioned in section IIa, an internal degree of freedom is attributed to each molecule by allowing the spheres representing the molecules to change their sizes. The characteristic frequency of the internal motion is controlled by the parameters of the anharmonic potential ascribed to this degree of freedom as

$$U_R = k_1\Delta R_i^2 + k_2\Delta R_i^3 + k_3\Delta R_i^4 \quad (3)$$

where $\Delta R_i = R_i - R_i^0$ is the deviation of the radius of the ith molecule from its equilibrium value R_i^0. The rate of the intermode energy transfer (primarily vibrational) is determined by the size of the anharmonicity and frequency mismatch between vibrational modes.[31−33] Thus, the parameters of the internal potential can be used to control the coupling between internal molecular motion and phonon modes and to achieve a desired rate of energy transfer from an excited molecule.[27]

It is this approximate internal mode that makes our model unique. We can explicitly include how fast the energy from the laser irradiation transfers from the molecule (or its chromophore) to the remainder of the system. The rate of energy transfer can be either estimated from experimental data or modeled with atomistic molecular dynamics simulations.[34,35] The rate of energy transfer can, of course, be different for different components of heterogeneous samples.

(d) Excitation Modes. There are numerous proposed microscopic mechanisms for absorption of the laser energy by the substrate. We have chosen to initially model the processes associated with UV-MALDI. In this case, it is believed that the photon is absorbed by an electronic transition followed by internal conversion to vibrational energy.

The effect of laser irradiation is thus simulated by vibrational excitation of random molecules during the time of the laser pulse within the penetration depth appropriate for a given wavelength and material. The absorption probability can be modulated by Beer's law to reproduce the exponential attenuation of the laser light with depth. In this case the probability for a given molecule to be excited depends on the fluence of the laser pulse and the position of the molecule under the surface. Vibrational excitation is modeled by depositing a quantum of energy equal to the photon energy into the kinetic energy of internal vibration of a given molecule.

The laser properties are thus explicitly included in the model. The wavelength of the laser light determines how much energy goes into each excitation event. The attenuation depth at this wavelength determines the distribution of molecules to be excited. In the case of heterogeneous systems, the excited molecules can be unevenly distributed among the components. The pulse width determines the time over which the excitation events occur and the fluence determines the number of molecules that are excited.

Although the initial studies have been for vibrational excitation of molecules, it is also possible to examine the consequences of photochemical reactions.[9,10,36−39] Photofragmentation, when an excited molecule reacts photochemically and forms fragments, can be simulated within the model in two different ways. An instantaneous increase of the equilibrium radius, R_i^0, of an excited molecule can be used to represent an increase in the volume occupied by the reaction products. This increase of R_i^0 shifts ΔR_i to the repulsive part of the internal potential, eq 3, and creates a local pressure pulse in the vicinity of the excited molecule. The pressure pulse can then dissipate to the thermal energy of the irradiated volume or, at high fluence, convert to the translational energy of ablation. An alternative way of simulating a photofragmentation event is to replace the sphere representing a molecule to be excited with several smaller spheres representing the resulting photofragmented molecules. The advantage of this approach is that the fate of the fragments can be followed during the course of the MD simulation and their role in the ablation process can be analyzed.

(e) System. The initial system chosen for modeling is the organic solid or matrix used in the mass spectrometric UV-MALDI experiments.[27] Typical matrixes are acids containing aromatic π-electrons such as nicotinic acid, sinapic acid, and 2,5-dihydroxybenzoic acid. In this paper we present results from a 2D simulation of size 81 × 210 nm or 58 800 molecules and a 3D simulation of size 10 × 10 × 40 nm or 27 648 molecules. To date the physical pictures arising from the 2D and 3D simulations are the same, although specific numerical values may differ. In some instances we use the 2D simulations in order to obtain better statistics and a clearer visual picture of the ablation events.

Periodic boundary conditions in the direction parallel to the surface are imposed. These conditions simulate the situation in which the radius of the laser beam is large compared to the penetration depth so that the effect of the edges of a laser spot can be neglected. In other words, processes occurring in the center of the laser beam are being examined. The bottom molecules are held rigid in the case of the 2D model. More complex boundary conditions used at the bottom of the 3D model are described in ref 27.

The parameters in the model were chosen with organic solids in mind.[27] For matrix molecules with a mass of 100 daltons and an equilibrium radius R_i^0 of 1.4 Å, the predicted properties of a 3D molecular solid are as follows: sublimation energy of 0.63 eV, elastic bulk modulus of ∼5 GPa, density of 1.2 g/cm^{-3}, and vibrational spectrum with a single broad band centered at 45 cm^{-1} with a width of ∼50 cm^{-1}. These values are typical for molecular solids.[12]

As mentioned above, the proposed breathing sphere model allows one to easily incorporate other species. In the present work analyte molecules with a mass 20 times that of the matrix molecules and $R_i^0 = 10$ Å are introduced into the 2D model. Each analyte molecule replaces in this case 18 matrix molecules. The concentration of analyte molecules is less than 0.2% in these simulations. The positions for analyte molecules to be introduced are chosen at random, and the results for 10 runs with different initial configurations are averaged in order to obtain statistically significant data on the ejection of analyte molecules. Small adjustments of the random choice of positions were made to ensure a uniform distribution with depth over the 10 runs of analyte positions.

For the calculations presented in this paper the parameters of the internal potential and the inertia parameter M are chosen[27] to provide the characteristic time of the vibrational relaxation of an excited molecule to be on the order of 10 ps.[34] The spectral peak corresponding to the internal vibrations in this case is embedded into the high-frequency tail of the phonon spectrum for the 3D system.

(f) Laser Irradiation. The laser irradiation in the present work is simulated by vibrational excitation of random matrix molecules. The total number of photons entering the model solid during the laser pulse is determined from the laser power and the pulse width. In the 2D model the absorption probability is evenly distributed over a penetration depth of 32 nm. An exponential decrease of the absorption probability with depth in accordance with Beer's law is used in the 3D simulation as

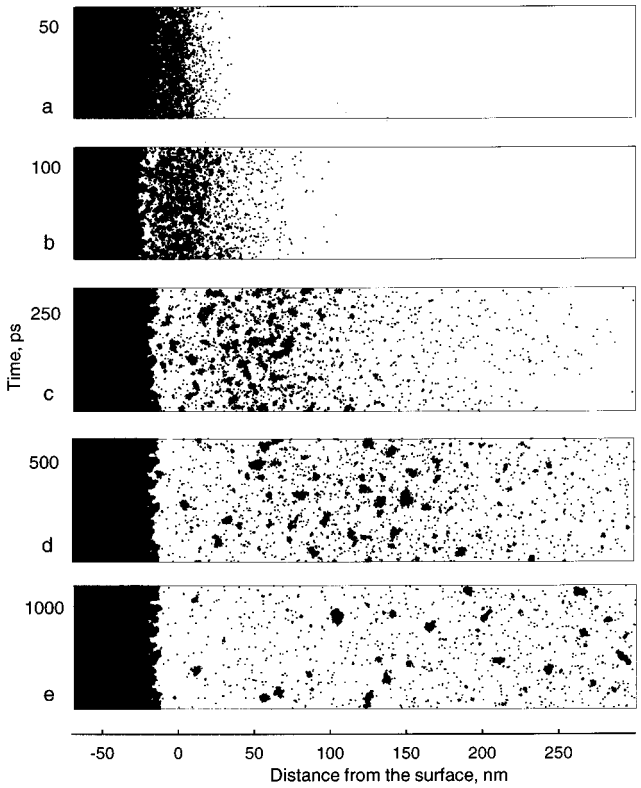

Figure 1. Time development of the plume for a 2D simulation. The total fluence is approximately twice the threshold fluence for ablation. The average energy deposited is 0.30 eV per particle in the irradiated region, whereas the cohesive energy is 0.31 eV. The pulse width is 15 ps.

qualitative comparisons with experimental data are made. A penetration depth of 7 nm is used in this case in order to provide an absorption of 99% of the laser energy within the computational cell. Laser pulses of 15 ps in duration at a wavelength of 337 nm (3.68 eV) are used in the simulations. The photon energy is scaled down by a factor of 2 for the 2D model in order to account for the lower cohesive energy of molecules in the 2D crystallite as compared to the 3D case.

III. Results

The results of the simulations are given in this section. First, we discuss the basic processes that distinguish ablation from desorption. Next, the time development of velocities and cluster composition within the plume is described. The last subsection discusses velocity distributions of both the matrix molecules and heavier analyte molecules.

(a) Physics of Ablation vs Desorption. The pictorial results from one 2D simulation in which ablation occurs are shown in Figure 1. The bulk of the sample is not shown but is to the left in the diagrams. The plume expansion is to the right. If the physics involved is straightforward desorption, then one would expect to see primarily individual molecules in the plume. This is clearly not the case for the plume shown in Figure 1.

To investigate the nature of the ablation phenomenon vs desorption, we calculated the desorption yields as a function of fluence for the 3D model. The total yield of molecules removed from the solid is plotted as a function of fluence in Figure 2. The yield increases at low fluences until point A where there is a jump in the yield to point B. Above this fluence the yield increases and appears to plateau at the highest fluences.

The calculations clearly show that the mechanism of particle removal below and above the points A and B is distinct. Below

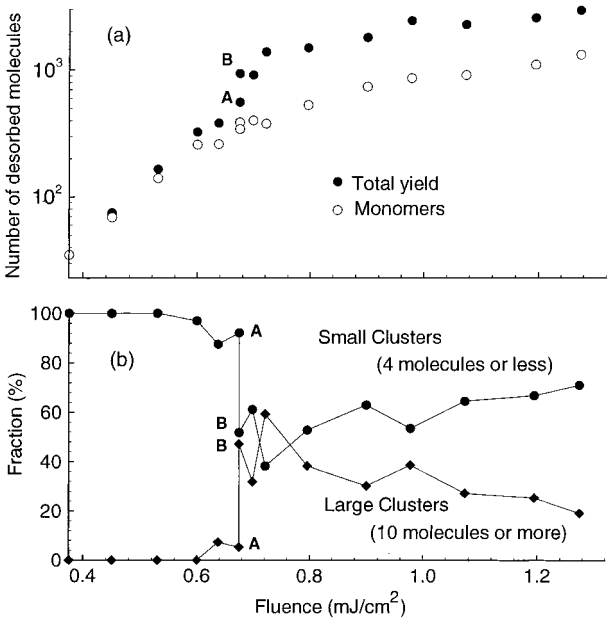

Figure 2. Desorption yield (a) and plume composition (b) vs fluence for the 3D simulation. Figure adapted from ref 28.

point A there is desorption that is characterized by events in which primarily individual molecules desorb as shown in Figures 2b and 3a. Above point B the ejected plume contains a substantial fraction of large molecular clusters as evidenced by Figures 2b and 3b. It is the presence of clusters of molecules in the plume that is primarily responsible for the jump in yield from point A to point B. The fluence dependence of the yield of individual molecules has no step increase (Figure 2a). The material removal at and above point B has an apparent collective character. Following the terminology that has been established,[2,17,40,41] we refer to this collective ejection process as ablation.

The physics leading to ablation is clearly delineated by the simulations.[28] Initially the laser energy is deposited into the internal breathing mode. This energy is transferred to thermal energy of translational motion of the molecules in the system and thus increases the temperature. The temperature rise is faster than mechanical relaxation in the system, thus a nearly constant volume heating occurs and the pressure increases. When the pressure gradient in the direction normal to the surface exceeds the mechanical strength of the material, it causes spallation and forwarded ejection of a significant part of the irradiated region. Near threshold this breakup or spallation of material due to the pressure buildup leads to ablation of large molecular clusters as shown in Figures 2b and 3b and costs the least energy per molecule ablated.

In addition to the pressure buildup due to inertial confinement, the rapid increase of the thermal energy can lead to an overheating of the system much beyond the boiling point. There are a number of important consequences of the overheating. First, when the system is heated close to the critical temperature, it undergoes a phase explosion (explosive boiling) in which the matrix decomposes into a gaseous mixture of individual molecules and clusters of molecules.[28] The fraction of individual molecules is related to the degree of overheating[23,42] and increases with laser fluence.[28] Second, the phase explosion increases the pressure that has already builtup due to the constant volume heating of the solid. Third, the phase explosion provides fast cooling of the ejected plume and short time of the thermal spike as discussed in the next subsection.

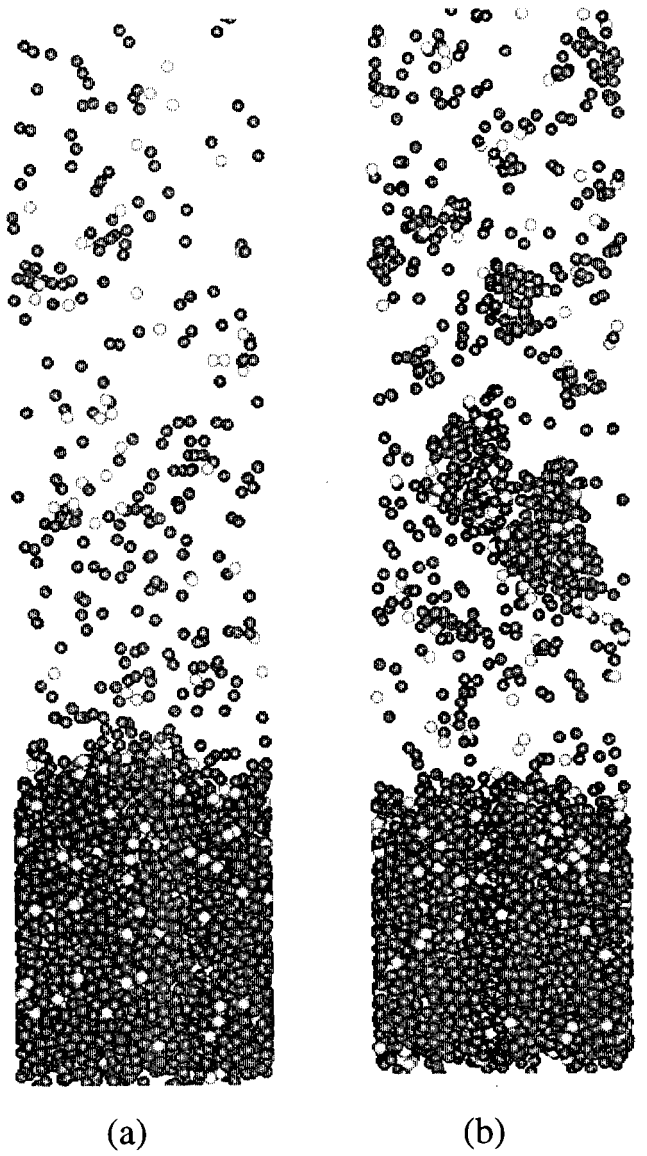

Figure 3. Snapshots of plume for the simulations at points A and B of Figure 2. The light spheres represent molecules that were excited by photon absorption.

At no point in the simulations did we assume that mechanical fracture or an explosive phase transition would occur. Rather they occurred as a consequence of a set of physical conditions appropriate for laser irradiation of the system.

(b) Plume Development. Examination of Figure 1 suggests that to describe the development of the plume, one should consider motion in the radial direction (parallel to the surface), the expansive motion in the axial direction, and cluster composition. We start with the radial velocities and the clusters.

Before discussing the time dependence of the radial kinetic energy, we would like to point out that the simulation results favor the association of the radial velocities with the thermal motion in the plume. As shown in the next subsection, the radial velocities of the ejected molecules have no significant correlation with the initial position under the surface and fit well to a Maxwell−Boltzmann distribution.

Our discussion starts with the short-time development of the averaged radial kinetic energy of a top part of the irradiated sample as shown in Figure 4 for four 2D simulations. These simulations range from the desorption regime to a fluence about twice the ablation threshold. Examining first the high fluence

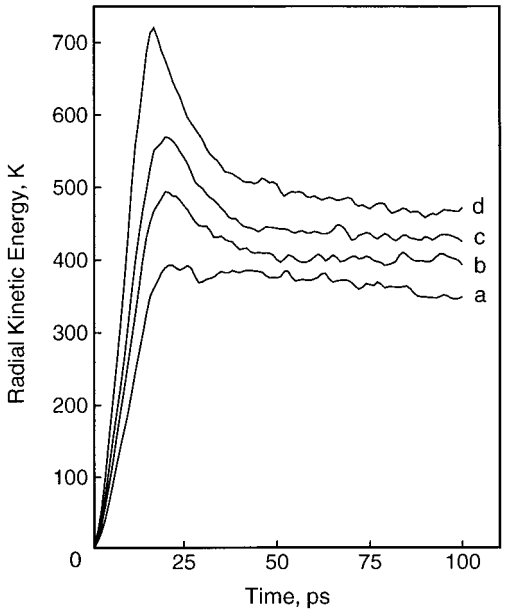

Figure 4. Averaged radial kinetic energy of the top 24 nm of the irradiated sample vs time for the 2D simulations at four different fluences. (a) Below the ablation threshold. (b) At the ablation threshold. (c) 1.4 times the ablation threshold. (d) Twice the ablation threshold. Curve d resulted from the simulation shown in Figure 1.

simulation, curve (d), the radial kinetic energy rises nearly linearly during the 15 ps laser pulse. The radial kinetic energy then rapidly drops for the next ∼25 ps. In this simulation the whole region over which the energy is averaged ablates and the fast cooling of the ablation plume is due to the phase explosion of the overheated matrix. A big part of the thermal energy is transferred in this case into potential energy of matrix decomposition and kinetic energy of the phase explosion and forwarded ejection. When less energy is deposited, a smaller degree of overheating is reached by the end of the laser pulse and a less violent explosion occurs. As a consequence, the temperature maximum is lower and the temperature drop is less dramatic, curves (b) and (c). Curve (a) in the figure is for the case of desorption, where the majority of the particles over which the average has been made remain in the target. No phase explosion occurs in this case, and the matrix cools slowly due to the evaporation and thermal conduction into the bulk of the sample. Of interest is similarity of the curves in Figure 4 to the temperature profiles predicted in ref 43 for the phase explosion model for ion bombardment desorption/ablation.

After the precipitous temperature drop shown in Figure 4d, the temperature continues to decline as shown in Figure 5. This decrease in temperature is directly related to decomposition and evaporation of molecular clusters. This is shown pictorially in Figure 1 and quantitatively in Figure 5b. As time increases, the number of molecules in large clusters decreases while the number in small clusters (including individual molecules) increases. Clearly the clusters of molecules are continuing to evaporate and the temperature continues to decrease beyond the end of the simulation.

The clusters, however, will not completely evaporate to individual molecules. For the simulation shown in Figures 1 and 5 the total energy deposited is 0.30 eV per molecule in the irradiated region. The cohesive energy is 0.31 eV. Moreover, some of the deposited energy has been converted to kinetic energy of molecules in the plume including the flow energy discussed below, and some is left as heat in the solid. Thus, there is insufficient energy to completely vaporize the ablated

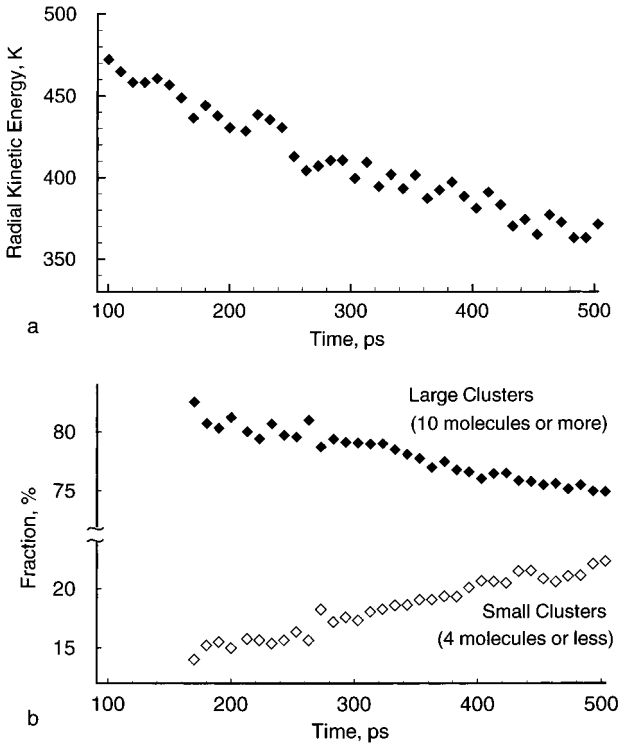

Figure 5. (a)Radial kinetic energy vs time for curve d of Figure 4 extended to longer times. (b) Cluster composition in the plume vs time. Shown is the percentage of molecules in small (four molecules or less including individual molecules) clusters and large (10 molecules or more) clusters. The partitioning between small and large is arbitrary, and any choice of small and large will exhibit the same trend. The data points are not presented for times earlier than 150 ps since the plume is too dense to define clusters; see Figure 1.

plume to individual molecules and clusters remain as a major integral part of the ejected plume. Note that in the simulation clusters are not formed within the ablation plume due to coalescence of gaseous species but arise naturally in the course of mechanical fragmentation and phase explosion, as discussed in the previous subsection.

Before proceeding to the axial velocities, there are a couple of observations. First, the melting temperature of the 2D system is about 400 K. It is clear from Figure 4 that the system does, in fact, overheat. Second, the system remains in this overheated state for a short period of time. Could this short overheating period contribute to the observation that the large molecules in MALDI remain intact? It is not possible to tell from these simulations whether the internal degrees of motion are equilibrated with the translational motion. What the simulations do point out is that to understand the ablation of large, intact biological molecules, the consequences of fast heating and cooling of the translational degrees of motion on the internal temperature must be understood.

We next turn our attention to the axial velocities. The data presented below are the result of the averaging over 10 simulations in which analytes are included. The fluence is nominally the same as that used for Figures 1 and 4d.

The time development of the axial velocities in the plume is shown in Figure 6a for molecules that originate from different depths below the surface. It is obvious that collisions among the ejected molecules lead to the redistribution of the energy and momentum in the axial direction and affect the final velocity distribution. The average axial velocity of the molecules that ablate from near the bottom of the plume decreases with time. On the other hand, the average axial velocity of the molecules

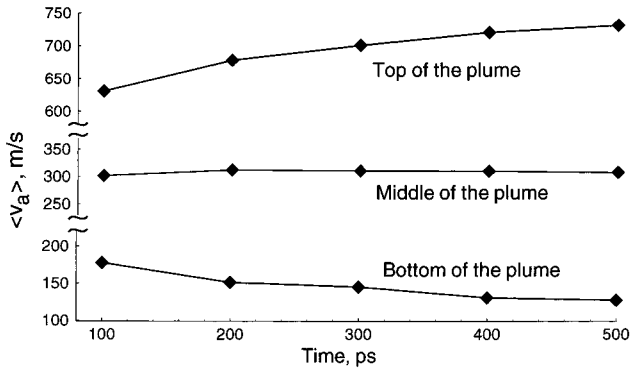

Figure 6. Average axial velocity vs time for (a) molecules from the four top monolayers, (b) molecules originally located at 12 nm under the surface, and (c) molecules originally located at 22 nm under the surface.

originating from the upper surface layers increases with time. This acceleration contributes to the high maximum velocities and leads to the high-velocity tail in axial velocity distribution as shown in the next subsection. Of note is that the axial velocity is concurrently being cooled due to evaporation of clusters as is the case for the radial velocity (Figure 5a). This effect is hidden by the energy redistribution due to collisions in the axial direction.

(c) Velocity Distributions. For laser ablation applications in mass spectrometry and film synthesis by pulsed laser deposition, the velocity distribution of the ablated molecules is an important characteristic for determining the resolution of the mass spectra or the structural quality of the deposited film. The measured velocity distributions are generally fit to a Maxwell−Boltzmann distribution function on a stream or flow velocity.[26,44−49] Equilibration in the moving reference frame is assumed to occur, and T is the equilibrium temperature of the plume. An additional fitting parameter, namely, the stream velocity u allows reasonably good fits of the experimental distributions observed in laser ablation experiments for a variety of systems such as molecular solids,[26,44] polymers,[46,50] frozen gases,[47] insulators,[48] and metals.[49]

The problems, however, arise when one wants to correlate the temperatures and stream velocities from the fit with real physical quantities of the system. The association of the spread of translational energy along the direction of flow solely with the thermal motion can be misleading and yields an overestimated value for translational temperature.[47,51] Moreover, angle-resolved measurements reveal that velocity distributions for off-normal angles could not be fit unless the parameters T and u are chosen to be dependent on angle.[26,48,52]

The pressure-driven ablation leads to different ejection conditions for molecules depending on their original depth in the substrate. Moreover, as shown in Figure 6, molecules originally at the top of the solid tend to get accelerated during the plume expansion and those at the bottom get decelerated. Consequently, we plot the average axial and radial velocity components of the ejected molecules as a function of their initial position under the surface in Figure 7. Each point in Figure 7 represents an average over molecules that belong to a four-monolayer-thick slab of material in the original system. For the entire depth of material ejected, there is nearly a linear dependence of the mean axial velocity on the initial position under the surface. This observation suggests that the single flow velocity as previously assumed is a rather poor approximation. Actually, there is a range of stream velocities from zero up to a maximum value.

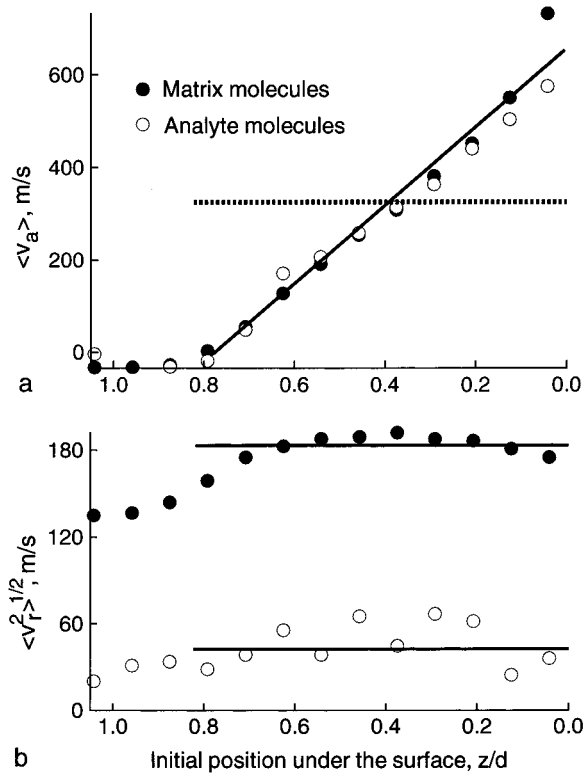

Figure 7. Average velocities of matrix and analyte molecules as a function of depth below the surface. (a) Axial velocity. The solid line represents the approximation of a range of stream velocities from zero to $u_{max} = 650$ m/s. The dashed line shows the approximation of a single stream velocity. (b) Radial velocity. Both lines represent a temperature of 400 K albeit for the two different masses of particles.

In contrast to the axial velocities, the radial velocities of the ejected matrix molecules have no significant correlation with the initial position under the surface. A root-mean-square radial velocity of 182 m/s, denoted by the solid line in Figure 7, corresponds to a temperature of 400 K.[53]

The results of molecular dynamics simulations discussed above suggest that the total velocity distribution in laser ablation can be described by one temperature but a range of stream velocities. Accordingly, we have modified the Maxwell−Boltzmann distribution with a single stream velocity, u, to one in which there is a range of stream velocities from zero to u_{max}.[29] The total velocity distribution of ejected molecules is then given by

$$dN(v,T,u_{max}) = \frac{m}{4\pi kTu_{max}} \exp\left\{-\frac{m(v_x^2 + v_y^2)}{2kT}\right\} \times \left\{\mathrm{erf}\left[\sqrt{\frac{m}{2kT}}v_z\right] - \mathrm{erf}\left[\sqrt{\frac{m}{2kT}}(v_z - u_{max})\right]\right\} dv_x\, dv_y\, dv_z \quad (4)$$

where erf is the standard error function, m is the mass of the particle, v_x, v_y, v_z are velocity components, and k is Boltzmann's constant.

The velocity distributions given by eq 4 for $T = 400$ K and $u_{max} = 650$ m/s are shown in Figure 8. The radial velocity distribution is well represented by a Maxwell−Boltzmann distribution at $T = 400$ K. The same temperature with a maximum stream velocity of 650 m/s ensures a good representation of the axial velocities as well. A fit of the axial velocity data in Figure 8 to a Maxwell−Boltzmann distribution function on a single stream velocity, on the other hand, results in a temperature as high as 1000 K and an average stream velocity of ∼325 m/s.

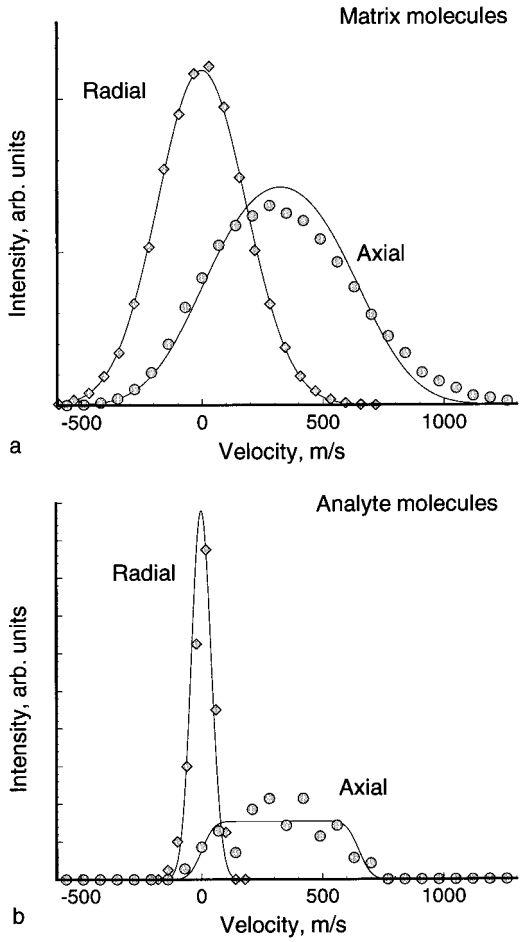

Figure 8. Velocity distributions in the axial and radial directions. The points are data from the simulation and the curves are obtained using eq 4 with $T = 400$ K and $u_{max} = 650$ m/s.

The two parameters of the proposed equation are independent of angle and have clear physical meaning, namely, the temperature that describes the thermal motion in the plume and the maximum stream velocity or velocity of the plume propagation in the direction normal to the surface. A discussion of the restrictions of this equation is given in ref 29.

The average axial and radial velocities of the analyte molecules are also given in Figure 7. The average axial velocities of the large, analyte molecules are virtually identical to the matrix molecules. In agreement with experimental observations,[25,44,54] the simulations show that the large molecules are entrained within the plume of the matrix molecules at nearly the same axial velocities. The only exception is for analyte molecules near the surface. Collisions between the lighter matrix molecules and the heavier analyte molecules are not as effective in accelerating the analyte molecules to the highest maximum velocities as for the matrix molecules. The average radial velocities of the analyte molecules display the same depth independence as the matrix molecules, but the value is reduced by $\sim\sqrt{\text{mass ratio}}$. The analyte molecules thus exhibit the same temperature.

The velocity distributions from the simulations of the analyte molecules are shown in Figure 8b. The distributions from our modified Maxwell−Boltzmann distribution, eq 4, are given for the same parameters as in the case of distributions for matrix molecules, $T = 400$ K and $u_{max} = 650$ m/s. Although the

statistics for the analyte molecules are limited, the agreement is clear. The good fit of the radial velocity distribution for both the matrix molecules and analytes indicates that nearly complete thermalization of translational molecular motion occurs between matrix and analytes in the ablation process. The flat-top shape of the axial velocity distribution in Figure 8b suggests that the spread in the axial velocities of analytes is due to the entrainment into expanding matrix, and the thermal motion does not significantly affect the distribution.

The velocity distributions of the neutral matrix and analyte molecules have been measured by laser postionization.[44] They obtain nearly identical matrix (ferrulic acid) and analyte (Gramicidin S) velocity distributions with a most probable velocity of ~400 m/s. The main difference in the experimental velocity distribution is that the matrix distribution has a tail that extends to higher velocities than the analyte distribution. This is completely understandable given the distributions in Figure 7. The matrix molecules that desorb from near the surface obtain larger velocities than any of the analyte molecules. It is these molecules that contribute to the high-velocity tail as seen in Figure 8. The majority of the analyte molecules do have the same velocity distribution as the matrix molecules. Most other measurements[25,54] of velocity distributions have been for ions, and the comparison with our simulations is not as direct.

The angular distributions follow naturally from the velocity distributions. Since the axial velocity contains a stream component whereas the radial velocity does not, the polar angle distribution will be forward peaked.[51,52,55,56] Moreover, since the axial velocity distribution of the matrix and analyte molecules are identical whereas the radial distributions differ by $\sim\sqrt{\text{mass ratio}}$, it follows naturally that the angular distribution of the analyte molecules will be more strongly forward peaked as has been noted in experiment.[56]

IV. Future Prospects

A comprehensive picture of the nature of the ablation process and plume development has emerged from molecular dynamics simulations using the breathing sphere model. Of note is that only the properties of the material and the laser characteristics are input to the calculations. There are no assumptions made a priori about mechanical fracture or overheating leading to ablation. Rather these events arise naturally from the simulations. Likewise no assumptions are made a priori about the correspondence of radial velocity with temperature and a range of stream velocities in the axial direction. Again, these concepts arise directly from the same calculations that predict the basic processes in the ablation phenomena.

The most exciting aspect of the model is the wide open door for future studies. One can easily conceive of the following simulations. (a) Other laser excitation processes such as photoablation can be compared to vibrational excitation. In particular, how is the physics different in the two situations and what are the ramifications on measurable quantities such as velocity distributions? (b) Other geometrical configurations of sample such as aerosol particles[57] and substrate-assisted laser desorption[58] are readily accessible for modeling.[59] (c) Complex and inhomogeneous materials in which the laser irradiation is absorbed by only one component[21,30,60,61] have a plethora of applications. (d) An interesting challenge is to modify the boundary conditions so that they can effectively absorb the laser-induced pressure waves.[61] This is necessary to be able to examine collateral damage or effects at the edges of the laser beam and to extend the simulations to longer times. (e) Models for ionization schemes can be incorporated into the simulation in order to examine the ramifications of charge on the final properties such as velocities.[16]

Acknowledgment. We gratefully acknowledge financial support from the National Science Foundation and the Office of Naval Research through the Medical Free Electron Laser Program. The computational support for this work was provided by the IBM-Selected University Research Program and the Center for Academic Computing at Penn State University. We appreciate helpful discussions with R. Srinivasan, R. F. Haglund Jr., D. D. Dlott, R. J. Levis, F. Hillenkamp, K. A. Prather, Y. Zhiltsova, J. Smirnova, and T. A. Schoolcraft.

References and Notes

(1) See, for example: *Radiat. Eff. Def. Solids* **1997**, *141*−*2*.
(2) Haglund, R. F., Jr. *Appl. Surf. Sci.* **1996**, *96*−*98*, 1.
(3) Karas, M. In *Fundamental Processes in Sputtering of Atoms and Molecules (SPUT 92);* Sigmund, P., Ed.; Det Kongelige Danske Videnskabernes Selskab: Copenhagen, 1993; p 623.
(4) Kotake S.; Kuroki M. *Int. J. Heat Mass Transfer* **1993**, *36*, 2061.
(5) Bencsura A.; Vertes A. *Chem. Phys. Lett.* **1995**, *247*, 142.
(6) Bencsura A.; Navale V.; Sadeghi M.; Vertes A. *Rapid Commun. Mass Spectrom.* **1997**, *11*, 679.
(7) Herrmann R. F. W.; Gerlach J.; Campbell E. E. B. *Nucl. Instrum. Methods Phys. Res. B* **1996**, *122*, 401.
(8) Herrmann R. F. W.; Gerlach J.; Campbell E. E. B. *J. Phys. B*, in press.
(9) Garrison, B. J.; Srinivasan, R. *J. Appl. Phys.* **1985**, *57*, 2909.
(10) Garrison, B. J.; Srinivasan, R. *Appl. Phys. Lett*. **1984**, *44*, 849.
(11) Garrison, B. J.; Srinivasan, R. *J. Vac. Sci. Technol. A* **1985**, *3*, 746.
(12) Kitaigorodsky, A. I. *Molecular Crystals and Molecules;* Academic Press: New York, 1993.
(13) *Proceedings of Laser*−*Tissue Interaction VII*; Jacques, S. L., Ed.; SPIE Proceedings Series 2681, **1996**; *Proceedings of Laser*−*Tissue Interaction VIII*; Jacques, S. L., Ed.; SPIE Proceedings Series 2975, **1997**.
(14) *Methods and Mechanisms for Producing Ions from Large Molecules;* Standing, K. G., Ens, W., Eds.; NATO ASI Series 269; Plenum Press: New York, 1991.
(15) Karas, M. *Biochem. Mass Spectrom.* **1996**, *24*, 897.
(16) Lowndes, D. H.; Geohegan, D. B.; Puretzky, A. A.; Norton, D. P.; Rouleau, C. M. *Science* **1996**, *273*, 898.
(17) Johnson, R. E. In *Large Ions: Their Vaporization, Detection and Structural Analysis*; Baer, T., Ng, C. Y., Powis, I., Eds.; John Wiley: New York, 1996; p 49.
(18) Vertes, A. In ref 10, p 275.
(19) Vertes, A.; Levine, R. D. *Chem. Phys. Lett*. **1990**, *171*, 284.
(20) Luk'yanchuk, B.; Bityurin, N.; Anisimov, S.; Malyshev, A.; Arnold, N.; Bäuerle, D. *Appl. Surf, Sci.* **1996**, *106*, 120.
(21) Venugopalan, V. In *Proceedings of Laser*−*Tissue Interaction VI;* Jacques, S. L., Ed.; SPIE Proceedings Series 2391, **1995**; p 184.
(22) Itzkan, I.; Albagli, D.; Dark, M. L.; Perelman, L. T.; von Rosenberg, C.; Feld, M. S. *Proc. Natl. Acad. Sci. U.S.A.* **1995**, *92*, 1960.
(23) Kelly, R.; Miotello, A. *Appl. Surf. Sci*. **1996**, 96−98, 205.
(24) Dreisewerd, K.; Schürenberg, M.; Karas, M.; Hillenkamp, F. *Int. J. Mass Spectrom. Ion Processes* **1995**, *141*, 127.
(25) Beavis, R. C.; Chait, B. T. *Chem. Phys. Lett.* **1991**, *181*, 479.
(26) Braun, R.; Hess, P. *J. Chem. Phys.* **1993**, *99*, 8330.
(27) Zhigilei, L. V.; Kodali, P. B. S.; Garrison, B. J. *J. Phys. Chem. B* **1997**, *101*, 2028.
(28) Zhigilei, L. V.; Kodali, P. B. S.; Garrison, B. J. *Chem. Phys. Lett.* **1997**, *276*, 269.
(29) Zhigilei, L. V.; Garrison, B. J. *Appl. Phys. Lett*. **1997**, *71*, 551.
(30) Edwards, G.; Logan, R.; Copeland, M.; Reinisch, L.; Davidson, J.; Johnson, B.; Maciunas, R.; Mendenhall, M.; Ossoff, R.; Tribble, J.; Werkhaven, J.; O'Day, D. *Nature* **1994**, *371*, 416.
(31) Banerjee, S.; Johnson, R. E.; Cui, S.-T.; Cummins, P. T. *Phys. Rev.* **1994**, *B43*, 12707.
(32) Zare R. N.; Levine, R. D. *Chem. Phys. Lett*. **1987**, *136*, 593.
(33) Zhigilei, L. V.; Srivastava, D.; Garrison, B. J. *Surf. Sci.* **1997**, *374*, 333.
(34) Chang T.-C.; Dlott, D. *J. Chem. Phys*. **1989**, *90*, 3590.
(35) Kodali, P. B. S. Ph.D. Thesis, The Pennsylvania State University, 1997.
(36) Srinivasan, R. In *Laser ablation, principles and applications*; Miller, J. C., Ed; Springer Series in Materials Science **28**, Springer-Verlag: Berlin, 1994; p 107.
(37) Tsuboi, Y.; Hatanaka, K.; Fukumura, H.; Masuhara, H. *J. Phys. Chem.* **1994**, *98*, 11237.

(38) Georgiou, S.; Koubenakis, A.; Syrrou, M.; Kontoleta, P. *Chem. Phys. Lett.* **1997**, *270*, 491.
(39) Borrmann, A.; Martens, C. C. *J. Chem. Phys.* **1995**, *102*, 1905.
(40) Haglund, R. F., Jr.; Kelly R. In *Fundamental Processes in Sputtering of Atoms and Molecules (SPUT 92);* Sigmund, P., Ed.; Det Kongelige Danske Videnskabernes Selskab: Copenhagen, 1993; p 527.
(41) Russo, R. E. *Appl. Spectrosc.* **1995**, *49*, 14A.
(42) Martynyuk, M. M. *Sov. Phys. Technol. Phys.* **1976**, *21*, 430.
(43) Sunner, J.; Ikonomou, M. G.; Kebarle, P. *Int. J. Mass Spectrom. Ion Processes* **1988**, *82*, 221.
(44) Huth-Fehre, T.; Becker, C. H. *Rapid Commun. Mass Spectrom.* **1991**, *5*, 378.
(45) Zhang, J.-Y.; Nagra, D. S.; Li, L. *Anal. Chem*. **1993**, *65*, 2812.
(46) Hansen, S. G. *J. Appl. Phys.* **1989**, *66*, 3329.
(47) Cousins, L. M.; Levis, R. J.; Leone, S. R. *J. Chem. Phys.* **1989**, *91*, 5731.
(48) Kools, J. C. S.; Baller, T. S.; De Zwart; S. T.; Dieleman, J. *J. Appl. Phys.* **1992**, *71*, 4547.
(49) Utterback, N. B.; Tang, S. P.; Frichtenicht, J. F. *Phys. Fluids* **1976**, *19*, 900.
(50) Srinivasan R.; Braren, B. *Chem. Rev*. **1989**, *89*, 1303.
(51) Ens, W.; Mao, Y.; Mayer, F.; Standing, K. G. *Rapid Commun. Mass Spectrom*. **1991**, *5*, 117.
(52) Jeffrey, W. E.; Levy, D. H. *J. Chem. Phys.* **1997**, *106*, 10368.
(53) The two-dimensional model has only one radial degree of freedom, thus the root-mean-square radial velocity of the particles is related to temperature by $\langle v_r^2 \rangle^{1/2} = (kT/m)^{1/2}$.
(54) Pan, Y.; Cotter, R. J. *Org. Mass Spectrom.* **1992**, *27*, 3.
(55) Spengler, B.; Bökelmann, V. *Nucl. Instrum. Methods Phys. Res. B* **1993**, *82*, 379.
(56) Zhang, W.; Chait, B. T. *Int. J. Mass Spectrom. Ion Proc*. **1997**, *160*, 259.
(57) Noble, C. A.; Prather, K. A. *Environ. Sci. Technol*. **1996**, *30*, 2667.
(58) Speir, J. P.; Amster, I. J. *Anal. Chem.* **1992**, *64*, 1041.
(59) Zhigilei, L. V.; Garrison, B. J. *Appl. Surf, Sci.*, in press.
(60) Wen, X.; Hare, D. E.; Dlott, D. D. *Appl. Phys. Lett.* **1994**, *64*, 184.
(61) Zhigilei, L. V.; Garrison, B. J. In *Proceedings of Laser−Tissue Interaction VI;* Jacques, S. L., Ed.; SPIE Proceedings Series 3254, in press.